34th Annual International Conference of the IEEE EMBS
San Diego, California USA, 28 August - 1 September, 2012

Decoding Arm and Hand Movements Across Layers of the Macaque Frontal Cortices

Yan T. Wong, *Member, IEEE*, Mariana Vigeral, David Putrino, David Pfau, Josh Merel, Liam Paninski, and Bijan Pesaran, *Member, IEEE*

Abstract— **A major goal for brain machine interfaces is to allow patients to control prosthetic devices with high degrees of independent movements. Such devices like robotic arms and hands require this high dimensionality of control to restore the full range of actions exhibited in natural movement. Current BMI strategies fall well short of this goal allowing the control of only a few degrees of freedom at a time. In this paper we present work towards the decoding of 27 joint angles from the shoulder, arm and hand as subjects perform reach and grasp movements. We also extend previous work in examining and optimizing the recording depth of electrodes to maximize the movement information that can be extracted from recorded neural signals.**

I. Introduction

For patients suffering from neurodegeneration, stroke, paralysis or upper limb amputation, there can be profound difficulties in communicating and interacting with the world. Currently there are many therapeutic devices that may provide some remedy to these issues. Such devices include visual search keyboards controlled via a cursor on a monitor [1], functional electrical stimulators to move paralyzed muscles [2], [3] and robotic arms and hands [4], [5].

To control these devices various interfaces have been proposed. These vary from non-invasive techniques such as tracking eye movements, foot switches, decoding electromyograms from remaining functional muscles or neural signals from scalp electrodes [6], to invasive techniques such as electrodes placed on the surface of the cortex [7] or penetrating the cortex [8], and electrodes implanted into reinervated muscles [9].

The benefit of the invasive techniques, in particular the brain machine interface (BMI), is that they offer the promise of signals with higher temporal and spatial fidelity. These signals have the potential to allow for the control of prosthetics with higher degrees of freedom.

*This work was sponsored by the Defense Advanced Research Projects Agency (DARPA) MTO under the auspices of Dr. Jack Judy through the Space and Naval Warfare Systems Center, Pacific Grant/Contract No. N66001-11-1-4205. BP was supported by a Career Award in the Biomedical Sciences from the Burroughs-Wellcome Fund, a Watson Program Investigator Award from NYSTAR, a Sloan Research Fellowship and a McKnight Scholar Award.

Y. W., M.V. D.P., and B. P. are with the Center for Neural Science, New York University USA

D.P., J.M., and L.P. are with the Statistics department at Columbia University.

Corresponding author: Bijan Pesaran: phone: 212-998-3578; fax: 212-995-4011; e-mail: bijan@nyu.edu).

Over the last decade, there has been great progress in brain machine interfaces [6–10]. However, as many prostheses aim to help patients suffering from upper limb paralysis or amputation, the number of independent degrees of freedom that current state-of-the art BMIs can control still falls well short of those exhibited in natural movement. For these invasive devices to be of full benefit to the end users, decoding strategies to control the many degrees of freedom in the arm, hand and shoulder are required.

Further, it has been long known that the functional organization of the neocortex changes across different cortical layers [14]. To maximize the efficacy and reliability of BMIs, the optimal depth at which electrodes need to be placed to record local field potentials (LFP) and spiking activity needs to be studied. In previous work, the optimal depth for decoding center-out saccadic movement goals from neuronal activity in the prefrontal cortex was found [15]. Future work is needed to determine whether neural recordings can be similarly optimized for the decoding of each joint angle involved in complex, unrestrained movements.

This paper presents neural decoding of 27 of the multiple degrees of freedom in the shoulder, arm and hand. In addition the paper examines how this information changes as a function of electrode recording depth in the cortex.

II. Methods

A. Experimental Preparation

One adult male Rhesus macaque (*Macaca mulatta*) participated in this study. Recording chambers were placed over dorsal premotor cortex (PMd) in both hemispheres. In each chamber, a thirty-two electrode semi-chronic microdrive was implanted (SC32-1, Gray Matter Research, USA). Electrodes were sharpened glass coated tungsten wires (Alpha Omega Inc., Il) and had initial impedance between 0.7 – 1.5 MΩ measured at 1 kHz. Electrodes had a center-to-center spacing of 1.5 mm and could be moved bi-directionally. Electrodes were advanced between 30-125 μm per recording session.

All surgical and animal care procedures were approved by the New York University Animal Care and Use Committee and were performed in accordance with the National Institute of Health guidelines for care and use of laboratory animals.

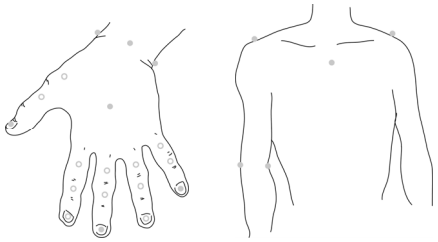

Figure 1 - Marker locations on the hand, arm and upper torso indicated by the grey circles. The full marker set is comprised of the filled and unfilled circle locations, while the reduced mark set is comprised of the just the filled circle locations.

B. Motion Tracking

The subject was tracked via reflective balls placed on the hand, arm and upper torso. The reflective balls were 3-mm in diameter and were illuminated and monitored using 16 infrared and near-infrared cameras (Osprey Digital RealTime System, Motion Analysis Corp., USA). Markers were placed in the middle of the distal, intermediate and proximal phalanges, and the back of the hand, (Fig. 1). Recordings were made with two different marker sets. In the full marker set, 24 markers were used (all circles, Fig. 1) and in the reduced marker set, markers were placed on the shoulders, elbow, wrists, and tips of the fingers (filled circles, Fig. 1). Movements were tracked at 200 frames/s and individual markers were identified offline (Cortex, Motion Analysis Corp.)

Once the marker data was labeled, joint angles in the hand, arm and shoulder were solved using a scaled musculoskeletal model of a Rhesus macaque right arm [16], [17] (SIMM, MusculoGraphics Inc., USA). For the full marker set, 27 joint angles were calculated, while in the reduced marker set 7 joint angles were calculated.

C. Behavioral Task

The subject performed reach-and-grasp movements to a range of spatial locations for liquid rewards. The subject was trained to grasp a small cube (25 mm x 25 mm x 25 mm, Fig. 2) on the end of a piece of dowel wood with a power grip. A reward was given for each correct grasp. The subject made reaches with his right limb.

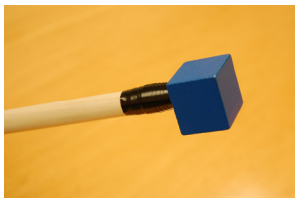

Figure 2 - Subjects were trained to reach to and grasp a cube. The cube was 25 mm on each side.

D. Offline Decoding Analysis

Joint angles were decoded from neural signals offline using a kernel-based autoregressive moving average (KARMA) model which nonlinearly maps population neural activity to dimensions of joint angles or arm motion [18]. Recording sessions were split into two equal halves and the model was fitted on one half and then used to decode the other half.

At time t, KARMA uses the past s neural states and past r arm position states to estimate the arm position at time $t + 1$. Let y_t be the arm position and x_t be the neural activity at time t. Let u_t be a vector which concatenates the r most recent arm position states ($y_{t-r+1:t}$) and the s most recent neural states ($x_{t-s+2:t+1}$). If the arm position is q dimensions, and there are d neural units, then u_t has dimension $sd + rq$. We train a support vector regression (SVR) model on input vectors u_t and the one-step-ahead output vectors y_{t+1}. After learning the support vectors v_i and the corresponding weights i from training data, we predict on separate data with the prediction function:

$$\hat{y}_{t+1} = \sum_i \alpha_i k(u_t, v_i)$$

with $k(\cdot,\cdot)$ the kernel function (we used a radial basis function). For our analyses, $r = s = 7$. When decoding a whole time-series, the $\hat{y}_{t+1}$ estimate will be part of u_{t+1} (real y_{t+1} is not known on non-training data). The neural data used has generally been 100 ms-binned firing rates (spikes determined by threshold-crossings) from the 64 electrodes (without spike sorting).

To characterize the performance of the predictions, the correlation coefficient between the actual joint angles and decoded joint angles was computed. All models and performance parameters were estimated through cross-validation. Finally, a neuron dropping analysis where decoding was performed with randomly permuted subsets of electrodes was used to examine the contribution of past arm states on decoding performance.

III. Results

One subject participated in 18 experimental sessions. We first present an analysis of the independence of joint angles during the behavioral task, then overall decoding performance of all joint angles, and finish with an analysis of how a decoding performance of a subset of joint angles changes with electrode recording depth.

A. Correlations in Joint Angles

To examine the complexity of the movements elicited in the behavioral task, the correlations between joint angles were calculated (Fig. 3). The joint angles in the shoulder were highly correlated with each other as well as the joint angles in the fingers. The high correlations in the fingers, especially in the ring, middle and index fingers, are resultant from all five fingers closing and opening around the target object in unison. Interestingly, joint angles in the wrist were negatively correlated to the joint angles in the fingers.

B. Decoding Joint Angles

Twenty-seven joint angles were decoded using recordings from all electrodes in both hemispheres from one session. Figure 4 presents the average correlation coefficient between the actual joint angles and the predicted joint angles for the KARMA decoding.

The average correlation coefficient in the shoulder, wrist and elbow for this one session was found to be 0.6 ± 0.1

(mean ± std.), while decoding joint angles in the fingers was poorer with a correlation coefficient of 0.5 ± 0.2.

When neurons were randomly sub-selected and used for decoding, performance increased from an average of 0.1 ± 0.1 (mean ± std.) for one electrode to 0.6 ± 0.2 for 64 electrodes (Fig. 5).

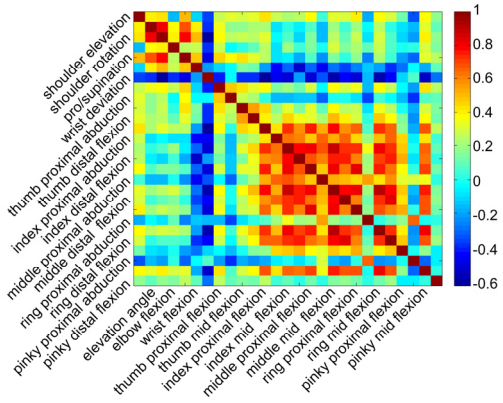

Figure 3 - Correlations between joint angles for the power grasp task. Labels for the odd rows and columns are presented to the left of the figure while labels for the even rows and columns are presented at the bottom of the figure. Joint angles in the fingers were highly correlated with each other.

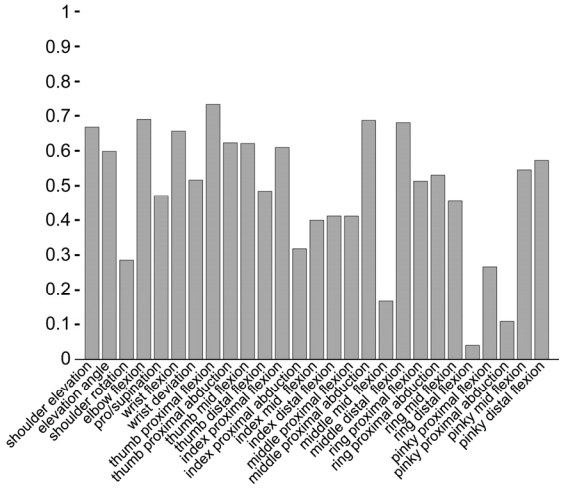

Figure 4 - Decoding performance from 64 electrodes across both hemispheres for the 27 degrees of freedom joint angles. Correlation coefficients between decoded and actual joint actions are presented.

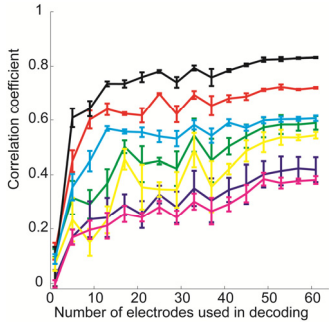

Figure 5 – Correlation coefficients (mean ± s.e.) for decoding with permutations of random subsets of electrodes. Decoding performance plateaus when more electrodes are added. (Red: shoulder elevation; green: shoulder elevation angle; blue: shoulder rotation; black: elbow flexion; yellow: pronation and supination; cyan: wrist flexion; magenta: wrist deviation.

C. Depth Decoding Performance

To examine the effects of neural recording depth on decoding performance, the average correlation coefficients for multiple recording sessions and different depths were analyzed. For this depth analysis a subset of seven joint angles in the shoulder elbow and wrist were used. Figure 6 presents the average decoding performace at different depths using the 32 electrodes in the left hemisphere (20 sessions; dashed lines) and using the 32 electrodes in the right hemisphere (20 sessions; solid lines). For electrodes in the left hemisphere there was an average of 10 ± 5 spiking channels in each session, while the electrodes in the right hemisphere had an average of 13 ± 5 spiking channels.

The average correlation coefficient across all joint angles and depths in the left hemishere was 0.4 ± 0.2 (mean ± std.), with better decoding performance from neural signals in the right hemisphere with an average correlation coefficient of 0.6 ± 0.2. Decoding performance was best for joint angles in the shoulder (left: 0.4 ± 0.1; right: 0.6 ± 0.1) and elbow (left: 0.4 ± 0.1; right: 0.6 ± 0.1) than for joint angles in the wrist (left: 0.3 ± 0.1; right: 0.4 ± 0.1). This trend was consistent for decoding of neural signals from the left and right hemisphere, and similar trends were observed with other decoders (e.g. Kalman filter), though we observed the best decoding performance using the KARMA model. The best decoding performance for the left hemisphere was at depth 1.5 mm (shoulder: 0.5 ± 0.2; elbow 0.7 ± 0.1; wrist: 0.4 ± 0.1). For the right hemisphere the best decoding performance was at 1.3 mm (shoulder: 0.7 ± 0.1; elbow: 0.8 ± 0.1; wrist: 0.6 ± 0.1).

Decoding performance in depth showed no clear trend across the left and right hemispheres. Using neural signals from the left hemisphere showed a stable decoding performance across depths and joint angles. However, decoding performance while using neural signals in the right hemisphere remained stable across most joint angles with the exception of shoulder rotation, pronation or supination and wrist deviation, which showed a gradual increase in decoding performance until a depth of 1.3 mm. More recording sessions at different depths need to be added to allow for a clearer examination of decoding performance in depth.

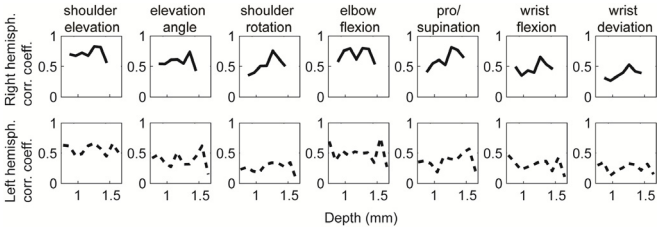

Figure 6 - Average decoding performance as a function of recording electrode depth for each microdrive. The correlation coefficients for actual and decoded joint angles are present in the top panels (solid lines) for the microdrive in the right hemisphere and bottom panels (dashed lines) for the microdrive in the left hemisphere.

IV. Discussion

This paper presents preliminary results in which a simple upper limb movement was tracked with high precision while recording neural activity bilaterally at multiple cortical depths. By analyzing the correlations in joint angles throughout the movements, we found that the joints in adjacent fingers moved in similar patterns during gross grasping tasks. These high correlations are not optimal in allowing the study of neural decoding of movements with high degrees of freedom. Future work will involve tasks that encourage individual finger movements to occur independently from each other, reducing the number of synergies in the movements.

With the current work, we decoded joint angles in the shoulder, wrist and elbow with a correlation coefficient of 0.6, while correlation coefficients for decoding joint angles in the fingers 0.5. The decreased decoding performance in the fingers may be due to increased noise in the joint angle solving in the distal bones. This noise arises from errors in the scaling of the bones in the hand and mismatches between actual and designated marker locations. Increasing the number of degrees of freedom involved in the behavioral task will increase the difficulty of the decoding resulting in a most likely decrease in accuracy. However, this may be offset by the addition of electrodes in other movement related areas such as ventral premotor and primary motor cortex.

Finally, when examining the effect of depth on the decoding of joint angles, no consistent trend was observed from the electrodes in the left and right hemispheres. An analysis of the neural data at more superficial recording depths may provide further insight into the encoding of individual joint angles. An accompanying analysis on the effect of each individual electrode site, through decoding with subsets of electrode groups, may allow for proper optimization across all 27 joint angles.

V. Conclusion

In this paper we present the decoding of 27 joint angles in a power grip task as well as the decoding performance of a subset of seven joint angles at different depths of the cortex. These preliminary results show that many degree of freedom movements can be decoded from neural activity. Future work will focus on increasing decoding performance through electrode number and placement and changes to task complexity.

Acknowledgement

The authors would like to thank Caroline Luk and Jessica Lasher for help with labeling the marker data, Dustin Hatfield and Phil Hagerman for help with motion tracking and Peter Loan for help with the rhesus macaque musculoskeletal model.

References

[1] G. Santhanam, S. I. Ryu, B. M. Yu, A. Afshar, and K. V. Shenoy, "A high-performance brain-computer interface.," *Nature*, vol. 442, no. 7099, pp. 195-8, Jul. 2006.

[2] P. H. Peckham, E. B. Marsolais, and J. T. Mortimer, "Restoration of key grip and release in the C6 tetraplegic patient through functional electrical stimulation.," *J Hand Surg*, vol. 5, pp. 462-469, 1980.

[3] K. L. Kilgore et al., "An implanted upper-extremity neuroprosthesis. Follow-up of five patients.," *J Bone Jt Surg (Am)*, vol. 79, no. 4, pp. 533-541, Apr. 1997.

[4] D.-P. Yang et al., "An Anthropomorphic Robot Hand Developed Based on Underactuated Mechanism and Controlled by EMG Signals," *J Bion Eng*, vol. 6, no. 3, pp. 255-263, Sep. 2009.

[5] S. C. Jacobsen, D. F. Knutti, R. T. Johnson, and H. H. Sears, "Development of the Utah artificial arm.," *IEEE Trans Biomed Eng.*, vol. 29, no. 4, pp. 249-269, Apr. 1982.

[6] J. R. Wolpaw, N. Birbaumer, D. J. McFarland, G. Pfurtscheller, and T. M. Vaughan, "Brain–computer interfaces for communication and control," *Clinical Neurophysiology*, vol. 113, no. 6, pp. 767-791, Jun. 2002.

[7] A. B. Schwartz, X. T. Cui, D. J. Weber, and D. W. Moran, "Brain-controlled interfaces: movement restoration with neural prosthetics.," *Neuron*, vol. 52, no. 1, pp. 205-220, Oct. 2006.

[8] L. R. Hochberg et al., "Neuronal ensemble control of prosthetic devices by a human with tetraplegia.," *Nature*, vol. 442, no. 7099, pp. 164-71, Jul. 2006.

[9] J. Yao, C. Carmona, A. Chen, T. Kuiken, and J. Dewald, "Sensory cortical re-mapping following upper-limb amputation and subsequent targeted reinnervation: a case report.," *Proceedings of 33rd Annual International Conference of the IEEE EMBS, Boston, USA*, vol. 2011, pp. 1065-8, Jan. 2011.

[10] M. A. Nicolelis, "Actions from thoughts.," *Nature*, vol. 409, no. 6818, pp. 403-407, Jan. 2001.

[11] A. K. Bansal, W. Truccolo, C. E. Vargas-Irwin, and J. P. Donoghue, "Decoding 3-D reach and grasp from hybrid signals in motor and premotor cortices: spikes, multiunit activity and local field potentials.," *J Neurophysiol*, Dec. 2011.

[12] R. Héliot, K. Ganguly, J. Jimenez, and J. M. Carmena, "Learning in closed-loop brain-machine interfaces: modeling and experimental validation.," *IEEE Trans Syst, Man, Cybern B, Cybern*, vol. 40, no. 5, pp. 1387-97, Oct. 2010.

[13] A. B. Schwartz, X. T. Cui, D. J. Weber, and D. W. Moran, "Brain-controlled interfaces: movement restoration with neural prosthetics.," *Neuron*, vol. 52, no. 1, pp. 205-220, Oct. 2006.

[14] D. Xing, C.-I. Yeh, and R. M. Shapley, "Spatial spread of the local field potential and its laminar variation in visual cortex.," *J Neurosci*, vol. 29, no. 37, pp. 11540-9, Sep. 2009.

[15] D. A. Markowitz, Y. T. Wong, C. M. Gray, and B. Pesaran, "Optimizing the Decoding of Movement Goals from Local Field Potentials in Macaque Cortex," *J Neurosci*, vol. 31, no. 50, pp. 18412-18422, Dec. 2011.

[16] S. L. Delp, J. P. Loan, M. G. Hoy, F. E. Zajac, E. L. Topp, and J. M. Rosen, "An interactive graphics-based model of the lower extremity to study orthopaedic surgical procedures.," *IEEE Trans Biomed Eng*, vol. 37, no. 8, pp. 757-67, Aug. 1990.

[17] S. L. Delp et al., "OpenSim: open-source software to create and analyze dynamic simulations of movement.," *IEEE Trans Biomed Eng*, vol. 54, no. 11, pp. 1940-50, Nov. 2007.

[18] L. Shpigelman, H. Lalazar, and E. Vaadia, "Kernel-ARMA for hand tracking and brain-machine interfacing during 3D motor control.," *Advances in Neural Information Processing Systems 21, NIPS, MIT press*, 2008.